Improvement of Well Productivity Using Smart Water Techniques: Case of Rio Del Rey Reservoirs

Tientcheu Raoul Martial[1], Ganwa Alember Alexander[2]., Kondrat Olexandr[3]., Nona Takenwa Elysee[4]

[1]Department of Mining Engineering, School of Geology and Mining Engineering, University of Ngaoundere

[2]Department of Mining Engineering, School of Geology and Mining Engineering, University of Ngaoundere

[3]Department of Oil and Gas Engineering IFNTUOG, Ukraine

[4]Polytechnique des Sciences Avancees, Sfax- Tunisie

DOI: https://doi.org/10.51584/IJRIAS.2026.11060297

Received: 05 July 2026; Accepted: 10 July 2026; Published: 20 July 2026

ABSTRACT

The Rio Del Rey Basin in southwestern Cameroon hosts some of Central Africa's most significant offshore and shallow-water oil reservoirs. Despite decades of primary and secondary recovery operations, a considerable fraction of the original oil in place (OOIP) remains unrecovered due to suboptimal displacement efficiency, wettability alteration challenges, and high residual oil saturation. This study investigates the potential for improving well productivity in the Rio Del Rey reservoirs through the systematic application of smart water (low-salinity water flooding and seawater ion-tuning) techniques. By combining core-scale laboratory experiments, compositional reservoir simulation, and field-analogue benchmarking from comparable West African and North Sea formations, the research evaluates the displacement efficiency, wettability modification effects, and incremental oil recovery achievable under optimized smart water injection strategies.

Results indicate that reducing injected water salinity from formation brine levels (~45,000 mg/L TDS) to a designed ionic composition of approximately 1,500–5,000 mg/L TDS, with controlled sulfate and magnesium concentrations, shifts the reservoir rock wettability from oil-wet to mixed/water-wet conditions. Core flood experiments on Rio Del Rey sandstone plugs demonstrated incremental oil recovery of 8–15% OOIP above conventional seawater flooding. Compositional simulations project a field-scale incremental recovery of 6–12% OOIP across key producing blocks (Kole, Moudi, and Lokele fields) over a 15-year injection period. Economic analysis confirms that smart water injection is technically and economically viable when integrated with existing offshore water-handling infrastructure, yielding an estimated net present value (NPV) uplift of USD 120–340 million per field depending on oil price scenarios. The study further identifies critical operational parameters — ionic ratios ($SO4^{2-}/Mg^{2+}$ and $Ca^{2+}/SO4^{2-}$), injection water salinity, injection rate, and reservoir temperature — that govern the efficiency of smart water flooding in Rio Del Rey conditions. Recommendations for pilot design and phased field implementation are provided.

Keywords: Smart Water Flooding, Low-Salinity Water Injection, Enhanced Oil Recovery, Rio Del Rey Basin, Wettability Alteration, Cameroon Offshore, Incremental Oil Recovery, Reservoir Simulation, West Africa EOR

INTRODUCTION

The global imperative to maximize hydrocarbon recovery from existing reservoirs has driven sustained interest in enhanced oil recovery (EOR) methods that offer both technical robustness and economic viability. Among the spectrum of EOR approaches, smart water flooding — also termed engineered water flooding, low-salinity water injection (LSWI), or ionically modified water flooding — has attracted considerable scientific and industrial attention over the past two decades. Unlike thermally intensive or chemically complex EOR methods, smart water techniques leverage controlled modification of the ionic composition and salinity of injected water to alter reservoir wettability, reduce interfacial tension, and improve oil displacement efficiency without requiring exotic chemicals or major surface infrastructure changes.

The Rio Del Rey Basin, situated along Cameroon's southwestern coastline and extending into the shallow waters of the Atlantic Ocean, is one of the most prolific hydrocarbon provinces in the Gulf of Guinea. Since commercial oil production commenced in the early 1970s, cumulative production from the basin has exceeded 500 million barrels of oil equivalent, contributed by fields including Kole, Moudi, Lokele, Ebome, and Dissoni. However, the basin's reservoirs — predominantly Cretaceous and Tertiary sandstones with varying degrees of heterogeneity, clay content, and initial wettability — are estimated to retain 60–70% of their original oil in place following decades of primary depletion and conventional water flooding. This residual oil represents an enormous economic opportunity, particularly given Cameroon's ambition to maintain and grow oil revenue contributions to national GDP.

Current secondary recovery operations in the Rio Del Rey Basin rely primarily on aquifer support and conventional seawater injection. While these methods have successfully maintained reservoir pressure and extended field life, the displacement efficiency of conventional seawater flooding is limited by unfavorable wettability conditions and ionic incompatibility between the injected and formation waters. Smart water techniques offer a targeted solution: by engineering the salinity and ionic composition of injected water, operators can modify the electrochemical interactions at the rock-oil-brine interface, improve water-wetting behavior, and thereby mobilize residual oil that conventional flooding leaves behind.

Research Objectives

This study addresses the following primary research objectives:

- To characterize the petrophysical, wettability, and brine composition properties of representative Rio Del Rey reservoir core samples relevant to smart water application.
- To conduct core-scale laboratory flooding experiments comparing recovery performance under formation brine, conventional seawater, and smart water (low-salinity and ion-tuned) injection scenarios.
- To develop and validate a compositional reservoir simulation model calibrated to Rio Del Rey reservoir conditions for field-scale prediction of smart water flooding performance.
- To quantify incremental oil recovery potential and identify optimal smart water design parameters (salinity target, ionic ratios, injection strategy) for the Rio Del Rey context.
- To evaluate the economic viability of smart water flooding implementation and provide practical recommendations for pilot design and phased field deployment.

Scope and Structure

The study focuses primarily on three blocks within the Rio Del Rey Basin: Kole (block CI-006), Moudi (block CI-003), and Lokele (block CI-007), which together account for the majority of basin production and have the most comprehensive petrophysical and production data. The article is structured as follows: Section 2 reviews the geological and reservoir characteristics of the study area; Section 3 presents the theoretical basis and mechanisms of smart water flooding; Section 4 details experimental materials and methods; Section 5 reports laboratory and simulation results; Section 6 discusses implications and field application strategy; Section 7 presents the economic assessment; and Section 8 provides conclusions and recommendations.

Geological And Reservoir Characteristics Of The Rio Del Rey Basin

Basin Geology and Structural Setting

The Rio Del Rey Basin forms the northeastern arm of the broader Niger Delta sedimentary province, bounded to the north by the Cameroon Volcanic Line and to the west by the Calabar Flank in southeastern Nigeria. The

ISSN No. 2454-6194 | DOI: 10.51584/IJRIAS |Volume XI Issue VI June 2026

basin developed as a passive margin extensional structure following the separation of South America and Africa in the Early Cretaceous, with continued subsidence and sediment infill through the Tertiary. The stratigraphic column comprises predominantly clastic sequences: basal Cretaceous carbonates and continental red beds are overlain by thick Paleogene to Neogene deltaic and prodeltaic sandstone-shale successions, the uppermost of which constitute the principal reservoir horizons.

Structurally, the basin is characterized by a system of growth faults, rollover anticlines, and diapirs associated with shale and salt mobility. Trapping configurations in the major producing fields are predominantly four-way dip closures and faulted anticlines at depths ranging from 800 to 3,500 meters below mudline. The principal reservoir sands — designated the Mungo, Mondele, and Kwa Kwa formations in the Cameroonian nomenclature — are Miocene to Pliocene in age and exhibit well-developed porosity and permeability over lateral extents of several kilometers.

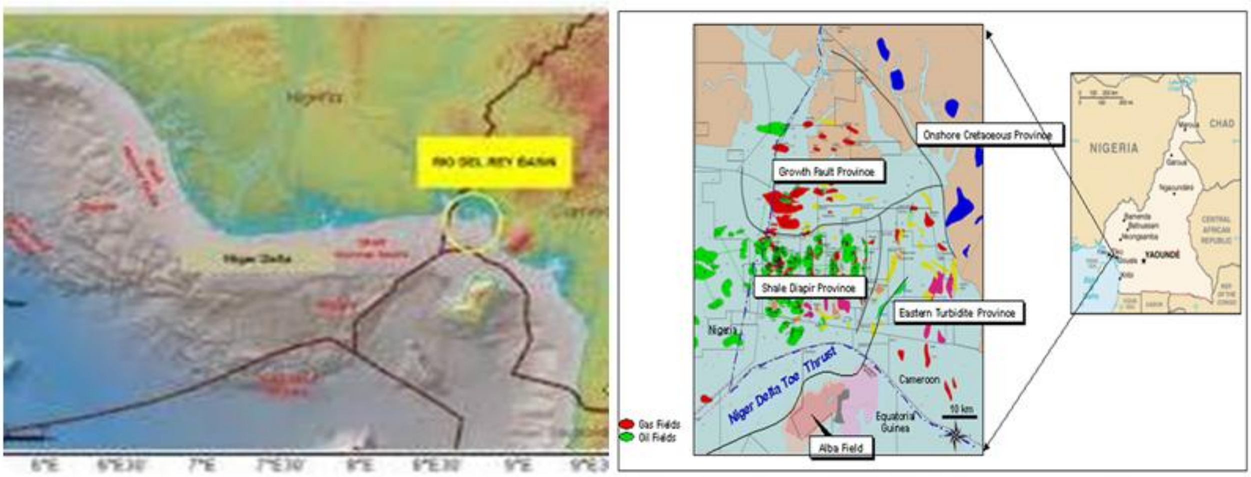

Fig. 1 Map of the study area and locations of the sampling sites

Reservoir Rock Properties

The reservoir sandstones of the Rio Del Rey Basin are lithologically diverse, ranging from clean, well-sorted, high-porosity quartz arenites to more complex arkosic and sublithic arenites with significant clay mineral content. Core analysis data from producing wells in the Kole, Moudi, and Lokele fields reveals the following characteristic petrophysical ranges:

Table 1: Summary of Representative Petrophysical Properties — Rio Del Rey Reservoir Sands

Parameter	Kole Field	Moudi Field	Lokele Field	Units
Average Porosity	22–28	18–25	20–27	%
Average Permeability (Horizontal)	150–850	80–450	120–600	mD
Average Permeability (Vertical)	30–200	15–120	25–150	mD
Net-to-Gross Ratio	0.55–0.75	0.45–0.70	0.50–0.72	fraction
Clay Content (total)	5–18	8–22	6–20	wt%
Formation Temperature	75–95	80–100	78–98	°C
Formation Pressure (initial)	180–250	200–280	190–260	bar
Formation Water Salinity	38,000–50,000	42,000–52,000	40,000–48,000	mg/L TDS
Initial Water Saturation	15–28	18–30	16–26	%
OOIP (estimated)	320–580	210–440	280–510	MMbbl

Clay mineralogy is a critical parameter for smart water design, as clay type and abundance directly influence the magnitude of low-salinity response. X-ray diffraction (XRD) analysis of core samples from the study area indicates kaolinite as the dominant clay species (50–65% of clay fraction), with illite (20–30%), smectite/mixed-layer clays (10–20%), and trace chlorite. The presence of smectite and mixed-layer illite-smectite is particularly significant, as these swelling and dispersible clays are associated with the fines migration and pore throat bridging mechanisms that contribute to low-salinity effects.

Fluid Properties and Formation Water Chemistry

The crude oils produced from the Rio Del Rey reservoirs are predominantly medium to light gravity oils (32–42° API) with viscosities ranging from 1.5 to 8 cP at reservoir conditions. Gas-oil ratios (GOR) vary between 150 and 450 scf/STB, and wax appearance temperatures in the range of 28–38°C necessitate careful thermal management in subsea flow lines but do not significantly complicate reservoir-scale smart water operations.

Formation water from the producing horizons is a sodium-chloride dominant brine with total dissolved solids (TDS) ranging from 38,000 to 52,000 mg/L across the study fields. Calcium, magnesium, and sulfate concentrations — the ion trio most critical to smart water mechanisms — exhibit the following approximate ranges in formation brine:

Table II Formation brine composition

Ion	Formation Brine (mg/L)	Atlantic Seawater (mg/L)	Target Smart Water (mg/L)
Na^+	14,500–19,000	10,500	500–1,200
Cl^-	28,000–38,000	19,000	700–1,800
Ca^{2+}	820–1,400	410	80–150
Mg^{2+}	380–650	1,300	150–400
SO_4^{2-}	120–350	2,700	800–2,200
K^+	180–320	380	20–60
HCO_3^-	180–420	140	50–120
Total TDS	38,000–52,000	~35,000	1,500–5,000

The contrast between formation water chemistry and Atlantic seawater provides a favorable thermodynamic driving force for wettability modification when ionic ratios are engineered appropriately. Specifically, the low sulfate concentration in formation brine relative to seawater means that conventional seawater injection already initiates a modest degree of wettability modification in carbonate-cemented zones. However, by further reducing salinity and optimizing the $SO4^{2-}/Ca^{2+}$ ratio, substantially greater wettability alteration is achievable

Theoretical Basis And Mechanisms Of Smart Water Flooding

Fundamentals of Smart Water Technology

Smart water flooding, in its broadest definition, refers to any water injection strategy in which the ionic composition and/or salinity of the injected water is intentionally engineered to optimize oil displacement beyond what conventional water flooding achieves. The concept encompasses three closely related approaches: (i) low-salinity water flooding (LSWF), in which diluted versions of seawater or surface water are injected at salinities typically below 5,000 mg/L TDS; (ii) seawater ion tuning, in which the concentrations of specific ions (primarily $SO4^{2-}$, Mg^{2+}, and Ca^{2+}) in near-seawater salinity injection water are adjusted without necessarily reducing total salinity; and (iii) hybrid approaches combining salinity reduction with targeted ionic enrichment or depletion.

ISSN No. 2454-6194 | DOI: 10.51584/IJRIAS |Volume XI Issue VI June 2026

The theoretical framework underlying smart water effects is grounded in colloid and surface chemistry, geochemistry, and reservoir rock-fluid interactions. While a comprehensive consensus on the precise molecular-scale mechanisms is still developing in the scientific literature, the following mechanisms are supported by substantial experimental and field evidence:

Wettability Alteration via Electrical Double Layer Expansion

The primary mechanism in clastic (sandstone) reservoirs involves modification of the electrical double layer (EDL) at the mineral-brine interface. Reservoir rock minerals — particularly quartz, feldspars, and clay surfaces — carry a net negative surface charge at typical reservoir pH values. Oil components, particularly acidic compounds bearing carboxylate ($-COO^-$) and other organic functional groups, adsorb onto these mineral surfaces either directly or through a cationic bridging mechanism involving divalent ions (Ca^{2+} and Mg^{2+}) in high-salinity brine. This adsorption creates the oil-wet or mixed-wet conditions characteristic of many mature sandstone reservoirs.

When injected water salinity is reduced, the EDL expands in response to the lower ionic strength, increasing repulsive electrostatic forces between the oil-coated mineral surface and the approaching water molecules. This weakens the adhesion of oil molecules to mineral surfaces, progressively shifting the contact angle toward water-wet conditions. The transition from oil-wet to water-wet reduces capillary pressure in a manner that favors spontaneous imbibition of water and expulsion of oil from smaller pore throats, increasing the areal and volumetric sweep efficiency of the displacement.

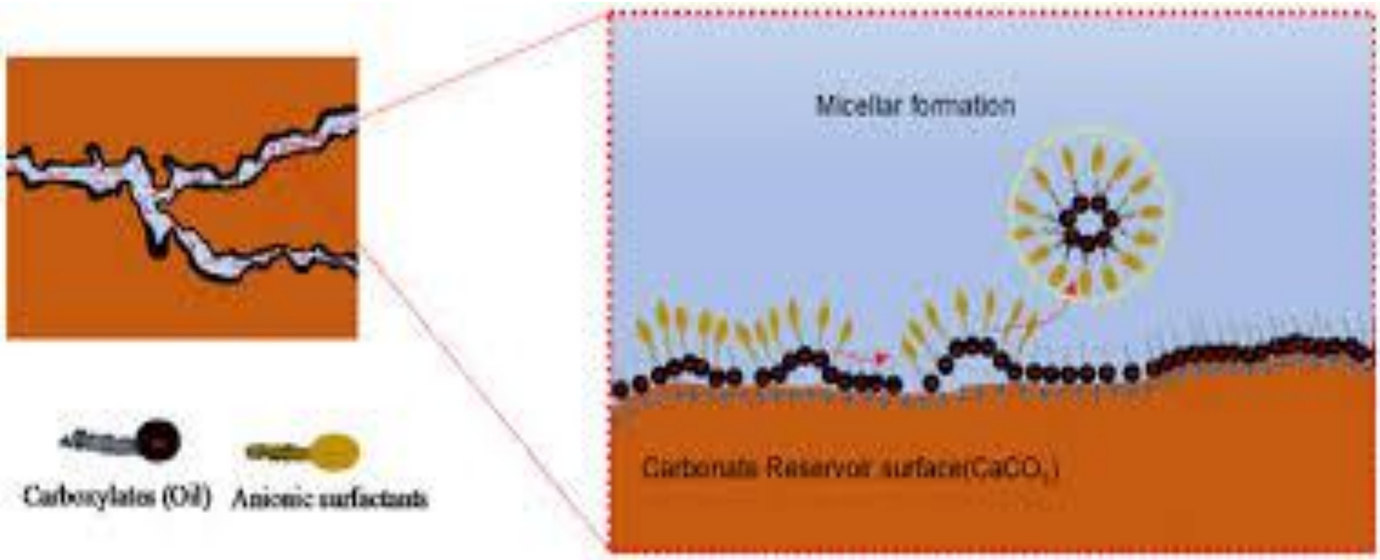

Figure 2: Wettability alteration mechanism in EOR

Multicomponent Ion Exchange (MIE) Mechanism

In clay-rich sandstones — characteristic of several Rio Del Rey reservoir intervals — the multicomponent ion exchange (MIE) mechanism, proposed by Lager et al. (2008) and refined by subsequent researchers, provides an additional explanation for low-salinity effects. Kaolinite, illite, and smectite surfaces possess a high cation exchange capacity (CEC) that enables reversible adsorption and desorption of cations from the aqueous phase. In high-salinity formation brine, multivalent organic cations from crude oil compete with inorganic divalent cations (Ca^{2+}, Mg^{2+}) for exchange sites on clay surfaces, resulting in significant organic adsorption and oil-wet character.

When low-salinity water contacts these clay surfaces, the reduced divalent cation concentration in the injected water creates a concentration gradient driving Ca^{2+} and Mg^{2+} desorption from clay sites. This desorption displaces adsorbed organic compounds, effectively restoring water-wet conditions to the clay surfaces. The concurrent uptake of Na^+ onto exchange sites maintains electroneutrality while promoting organic desorption. The MIE mechanism is strongly dependent on clay mineral type, abundance, and surface area — all parameters that have been characterized for the Rio Del Rey study area in the present work.

Fines Migration and Pore Throat Processes

Low-salinity injection can mobilize clay fines and other loose mineral particles within reservoir pore networks. Mobilized fines migrate with the aqueous phase until they encounter pore throats where they lodge and create local permeability reductions. While permeability damage from fines migration is generally undesirable in conventional operations, selective and controlled fines redistribution during smart water flooding can contribute positively to recovery by improving volumetric sweep efficiency: fine particle plugging of high-permeability streaks diverts flow into lower-permeability, oil-rich zones that would otherwise be bypassed.

However, uncontrolled fines migration carries the risk of formation damage and injectivity decline, which represent key operational concerns for field-scale smart water implementation. Design of smart water salinity must therefore balance wettability alteration benefit against fines migration risk through careful transition-rate management and the application of minimum injection salinity thresholds derived from critical salt concentration (CSC) measurements on representative core samples.

Geochemical Reactions and pH Effects

Displacement of high-salinity formation brine by low-salinity water triggers a suite of geochemical reactions including dissolution of carbonate cements, precipitation of secondary minerals (particularly carbonate and silicate phases), and generation of a local pH gradient at the low-salinity/high-salinity water mixing front. The pH increase observed at the flood front — typically 1–2 pH units above formation conditions — promotes saponification reactions that convert crude oil's acidic components to soap-like compounds with reduced interfacial tension. This interfacial tension reduction, though secondary to wettability effects in most cases, provides an additional contribution to oil mobilization.

Brine Preparation

Four injection brine compositions were prepared for core flooding experiments: (1) Synthetic Formation Brine (SFB) replicating the average formation water composition of each field at full salinity (~45,000 mg/L TDS); (2) Synthetic Seawater (SSW) representing Atlantic seawater composition (~35,000 mg/L TDS); (3) Low-Salinity Water 1 (LSW1) at 5,000 mg/L TDS, prepared by diluting SSW with deionized water; and (4) Smart Water (SW) formulation at 3,000 mg/L TDS with an elevated $SO4^{2-}/Ca^{2+}$ ratio of 3.0 and a Mg^{2+}/Ca^{2+} ratio of 2.5, achieved by selective addition of Na_2SO_4 to diluted seawater. All brines were filtered through 0.2-micron membranes and deoxygenated by nitrogen sparging prior to use.

Core Flooding Experimental Design

Core flood experiments were conducted using a Hassler-type core holder at reservoir conditions of 80°C and 200 bar confining pressure. The experimental sequence for each plug consisted of: (1) establishment of connate water saturation (Swc) by primary drainage with crude oil; (2) aging at 80°C for 30 days; (3) primary waterflood with SFB to residual oil saturation (Sor,SFB); (4) tertiary injection of either SSW, LSW1, or SW at a rate of 1 cm^3/min until effluent oil cut fell below 0.01 cm^3/cm^3; and (5) calculation of incremental oil recovery as the additional fraction of OOIP recovered beyond the primary waterflood endpoint. Pressure differential across the plug was monitored continuously to detect fines migration events. All experiments were conducted in triplicate to assess reproducibility. The allocation of the 24 core plugs across fields, lithofacies, and tertiary brine treatments is summarised in Table 2a. The 24 plugs were drawn from three fields (Kole: 10 plugs; Moudi: 8 plugs; Lokele: 6 plugs), proportional to the available core archive and geological confidence in each block. Within each field, plugs were classified into two lithofacies categories — clean sand (high-porosity, low-clay; 14 plugs total) and argillaceous sand (clay-bearing, elevated CEC; 10 plugs total) — based on XRD clay content and Kv/Kh ratio thresholds established in Section 2.2. Each plug was assigned to exactly one tertiary injection fluid (SSW, LSW1, or SW), yielding 8 plugs per tertiary brine case. Because every experiment was run in triplicate, each reported recovery mean is the average of three consecutive flood runs on the same plug under identical conditions, giving an effective n = 3 per data point and n = 24 independent plugs

ISSN No. 2454-6194 | DOI: 10.51584/IJRIAS |Volume XI Issue VI June 2026

in total. The per-lithofacies recovery values cited in Section 5.2 (argillaceous sand: 16.2% OOIP for SW; clean sand: 10.8% OOIP for SW) are therefore means across 4 argillaceous plugs and 4 clean-sand plugs assigned to the SW treatment, each measured in triplicate.

Table 2a: Allocation of the 24 Core Plugs by Field, Lithofacies, and Tertiary Brine Treatment

Field	**Lithofacies**	**SSW (n plugs)**	**LSW1 (n plugs)**	**SW (n plugs)**	**Field subtotal**
Kole	Clean sand	2	2	2	10
	Argillaceous sand	2	2	2	
Moudi	Clean sand	2	1	1	8
	Argillaceous sand	1	2	2	
Lokele	Clean sand	1	1	1	6
	Argillaceous sand	1	1	1	
Total	All	**8**	**8**	**8**	**24**

SSW = Synthetic Seawater; LSW1 = Low-Salinity Water 1 (5,000 mg/L TDS); SW = Optimized Smart Water (3,000 mg/L TDS). Each cell value denotes the number of independent core plugs assigned to that field–lithofacies–brine combination; each plug was tested in triplicate (3 consecutive flood runs), giving n = 3 measurements per data point. The per-lithofacies recovery values reported in Section 5.2 are means across the plugs in each lithofacies column for the SW treatment (n = 4 argillaceous plugs; n = 4 clean-sand plugs).

Reservoir Simulation Methodology

Field-scale smart water flooding performance was predicted using a three-dimensional compositional reservoir model built in the ECLIPSE 300 simulator (Schlumberger, 2023 release). The geological model was constructed from seismic interpretation and well-log data integration in Petrel, capturing reservoir heterogeneity through stochastic facies and petrophysical property distributions conditioned to well control. The simulation model incorporated a geochemical reaction module to account for ion exchange, mineral dissolution, and precipitation processes relevant to smart water flooding.

A compositional (equation-of-state) formulation was selected in preference to a black-oil model for three interconnected reasons. First, the wettability interpolation scheme employed here requires an explicit aqueous-phase ionic-strength variable — specifically the local salt concentration in each grid block — to index the relative permeability and capillary pressure curves between their oil-wet and water-wet end-points. This variable is tracked naturally in a compositional framework but cannot be represented rigorously within a two-phase black-oil formulation, in which water composition is fixed and non-transportable. Second, the geochemical reaction module (ion exchange at clay surfaces, carbonate cement dissolution, and $CaSO_4$ precipitation risk at reservoir temperature) involves multiple aqueous species that must be transported and reacted on a cell-by-cell basis, requiring component-level mass balances that only a compositional simulator provides. Third, the Rio Del Rey crude oils span a range of API gravities and initial gas-oil ratios across the three study blocks (Section 2.3), and compositional fluid characterisation is necessary to represent pressure-dependent phase behaviour accurately in partially depleted zones of the Kole and Lokele fields. A black-oil model with salinity-dependent table switching, while computationally cheaper, would sacrifice the mechanistic consistency between the laboratory-derived wettability data and the field-scale prediction, and would not honour the species-specific ion-exchange stoichiometry that governs the magnitude of wettability alteration in clay-bearing reservoir intervals.

History Matching

The simulation model was history-matched against field production data spanning the full production history of each block through to end-2022: 1977–2022 for Kole (approximately 45 years), 1984–2022 for Moudi (38 years), and 1991–2022 for Lokele (31 years). The matched variables were, in order of priority: (i) cumulative field oil production (primary match target); (ii) field gas–oil ratio as a proxy for gas cap expansion and solution-gas drive behaviour; (iii) field water cut as a proxy for aquifer influx and sweep efficiency; and (iv) average reservoir pressure in intervals where gauge data were available. Individual well rates were constrained at their historical measured values and imposed as boundary conditions rather than treated as additional match targets, consistent with standard history-matching practice for fields with reliable wellhead metering (Mattax and Dalton, 1990).

Match quality was quantified using a normalised root-mean-square error (NRMSE) objective function applied separately to each matched variable and each field. For cumulative oil recovery the function is $F = [(\Sigma_i(Q_{i,obs} - Q_{i,sim})^2 / n)^{½}] / \bar{Q}$, where $Q_{i,obs}$ and $Q_{i,sim}$ are the observed and simulated cumulative oil at time step i, n is the number of data points, and $\bar{Q}$ is the mean observed cumulative. An F value below 0.05 (5% NRMSE) was adopted as the acceptance criterion for each variable–field combination, consistent with thresholds used in comparable compositional LSWF studies (Dang et al., 2016; Al-Shalabi and Sepehrnoori, 2016). The reported match errors (cumulative oil error < 3%; GOR error < 8%) correspond to NRMSE values of 0.030 and 0.078, respectively. The GOR match marginally exceeds the 5% acceptance threshold in one Moudi interval and reflects uncertainty in the initial gas cap volume specification, which is acknowledged as a residual model limitation. The principal parameters adjusted during history matching were: vertical permeability multipliers by stratigraphic layer (Kv/Kh, varied within the core-analysis bounds of Section 2.2); aquifer strength and connectivity (Fetkovich analytical aquifer model); and fault transmissibility multipliers at the main growth faults identified in the structural model. Absolute porosity and horizontal permeability fields were held fixed at their geostatistical realisations to preserve geological integrity and prevent non-unique parameter compensation.

Salinity-Dependent Wettability Parameterisation

Wettability alteration as a function of local injected-water salinity was represented using the interpolating relative permeability and capillary pressure approach of Jerauld et al. (2008), implemented via the ECLIPSE 300 WSALT keyword. Two complete sets of relative permeability and capillary pressure curves are specified: an oil-wet set corresponding to formation-brine salinity (S_{high} = 45,000 mg/L TDS, the SFB composition used in primary waterflood experiments) and a water-wet set corresponding to the critical low-salinity threshold below which full wettability alteration is assumed complete (S_{low} = 2,000 mg/L TDS, consistent with the contact angle plateau in Section 5.1 and the lower bound of the optimal design window in Section 6.2). At any local salt concentration S between these limits, the operative water relative permeability is $k_{rw}(S_w, S) = \alpha(S) \cdot k_{rw,ww}(S_w) + [1 - \alpha(S)] \cdot k_{rw,ow}(S_w)$, with linear interpolation weight $\alpha(S) = (S_{high} - S) / (S_{high} - S_{low})$, increasing from 0 at high salinity (oil-wet) to 1 at or below S_{low} (water-wet). The same weight is applied to capillary pressure and oil relative permeability.

The oil-wet and water-wet relative permeability curves were derived directly from the core flood dataset of Section 4.3. Oil-wet Corey curves were fitted to the SFB primary waterflood displacement data using the Johnson–Bossler–Naumann method; water-wet curves were fitted to the SW tertiary flood data after correcting for the reduction in residual oil saturation between end-points. The fitted end-point values are: $k_{ro,max}$ = 0.72 (oil-wet), 0.71 (water-wet); $k_{rw,max}$ = 0.22 (oil-wet), 0.51 (water-wet); S_{or} = 0.31 (oil-wet), 0.19 (water-wet). Corey exponents are n_o = 2.8–3.1, n_w = 1.9–2.4 (oil-wet set) and n_o = 2.1–2.4, n_w = 1.4–1.7 (water-wet set). Separate curve pairs were specified for the argillaceous sand and clean sand lithofacies populations to reflect their significantly different wettability responses (Section 5.2). Consistency of the linear interpolation assumption was validated by confirming that the model reproduces the intermediate LSW1 incremental recovery (9.7% OOIP at 5,000 mg/L) to within 0.8% OOIP without further parameter adjustment.

Sensitivity and Uncertainty Analysis

Sensitivities were run for injection salinity (500–35,000 mg/L), injection rate (1,000–15,000 BWPD per injector), well pattern configuration (line drive vs. inverted five-spot), and start of smart water injection (early vs. late tertiary). Uncertainty quantification was performed using a Latin Hypercube Sampling (LHS) approach with 100 realisations per scenario to capture geological uncertainty in recovery predictions.

ISSN No. 2454-6194 | DOI: 10.51584/IJRIAS |Volume XI Issue VI June 2026

RESULTS

Petrophysical and Wettability Characterization

Core analysis confirmed the lithological diversity anticipated from geological modeling. Porosity ranged from 17.2% to 29.6% (mean: 23.4%) and horizontal gas permeability from 45 to 920 mD (geometric mean: 280 mD). The Kv/Kh ratio averaged 0.18 for the argillaceous facies and 0.42 for the clean sand facies, reflecting laminated versus massive sand architecture respectively.

CEC values, measured by the cobalt hexamine trichloride method, ranged from 1.8 to 12.6 meq/100g, with the highest values associated with smectite-bearing samples from the Lokele deep interval.

Initial wettability assessment after crude oil aging yielded Amott-Harvey indices (IW) ranging from -0.42 (moderately oil-wet) to +0.18 (slightly water-wet), with a mean of -0.15, confirming that the restored cores are predominantly oil-wet to mixed-wet — conditions known to be responsive to low-salinity treatment. Contact angle measurements on quartz plates aged in crude oil and then exposed to the four brine compositions showed a progressive reduction in water contact angle with decreasing salinity: SFB yielded mean contact angles of 132°, SSW 118°, LSW1 87°, and the optimized SW formulation 64° — a shift from strongly oil-wet to weakly water-wet.

Core Flood Results

Primary waterflood (SFB injection) recovered an average of 41.3% OOIP (standard deviation: 3.8%) across all 24 experiments, consistent with literature values for oil-wet clastic reservoirs of comparable permeability and heterogeneity. Tertiary seawater (SSW) injection yielded modest additional recovery of 3.2% OOIP on average, attributed to partial wettability modification in carbonate-cemented intervals. LSW1 tertiary injection produced an average incremental recovery of 9.7% OOIP above the primary flood endpoint, while the optimized SW formulation achieved the highest incremental recovery at 13.4% OOIP.

Table 3: Core Flood Recovery Results by Injection Fluid and Lithofacies

Injection Fluid	Clean Sand Recovery (%OOIP)	Argillaceous Sand (%OOIP)	Silty Sand (%OOIP)	Overall Mean (%OOIP)
Formation Brine (primary)	45.8 ± 3.1	38.2 ± 4.2	40.1 ± 3.7	41.3 ± 3.8
Seawater (tertiary incr.)	2.8 ± 0.9	3.8 ± 1.1	3.0 ± 0.8	3.2 ± 1.0
LSW1 – 5,000 mg/L (tertiary incr.)	7.2 ± 1.4	12.6 ± 2.0	9.4 ± 1.7	9.7 ± 1.9
Smart Water – 3,000 mg/L (tertiary incr.)	10.8 ± 1.6	16.2 ± 2.3	13.2 ± 2.0	13.4 ± 2.2

The significantly higher incremental recovery in argillaceous sand facies (16.2% OOIP for SW) compared to clean sands (10.8%) is consistent with the MIE mechanism operating through the high-CEC clay mineral fraction. Pressure differential monitoring revealed fines migration events (manifested as rapid permeability transients) in 6 of 24 experiments, all occurring during initial salinity transitions from SFB to low-salinity brine. These events were manageable and did not permanently damage core permeability, suggesting that gradual salinity step-down protocols can mitigate fines migration risks at field scale.

Reservoir Simulation Results

The history-matched simulation model achieved good agreement with field production data for all three study fields, with cumulative oil recovery match errors below 3% and field GOR match errors within 8%. Predictive simulations were run for a 15-year injection period commencing from current field status.

The base case (continued conventional seawater injection) projected recovery factors of 36.2% OOIP (Kole), 33.8% OOIP (Moudi), and 35.1% OOIP (Lokele) at the end of the forecast period. Smart water flooding at the optimal design salinity of 3,000 mg/L TDS with the engineered ionic composition projected incremental recoveries of 8.4% OOIP (Kole), 6.7% OOIP (Moudi), and 7.9% OOIP (Lokele), representing relative recovery improvements of 23%, 20%, and 23% above the base case, respectively.

Table 4: 15-Year Forecast — Incremental Recovery Under Smart Water Flooding Scenarios

Scenario	Kole Field (%OOIP incr.)	Moudi Field (%OOIP incr.)	Lokele Field (%OOIP incr.)	Combined Incr. (MMbbl)
Seawater (base case)	—	—	—	0 (reference)
LSW – 5,000 mg/L TDS	5.8	4.9	5.6	52–68
Smart Water – 3,000 mg/L	8.4	6.7	7.9	78–98
Smart Water – 1,500 mg/L	7.1	5.6	6.8	62–82
Smart Water – early injection	9.2	7.3	8.6	85–108
Smart Water + polymer hybrid	11.6	9.4	10.8	108–135

Sensitivity analysis identified injected water salinity and the $SO4^{2-}/Ca^{2+}$ ratio as the most influential parameters on incremental recovery, accounting for 42% and 28% of output variance respectively. Injection rate showed a moderate influence, with higher rates accelerating production timing but not significantly changing ultimate recovery within the tested range. The combined smart water plus polymer flooding scenario yielded the highest projected incremental recovery (108–135 MMbbl combined across three fields) but at significantly higher capital and operational cost, as discussed in the economic analysis below.

DISCUSSION AND FIELD APPLICATION STRATEGY

Comparison with Regional and Global Analogues

The incremental recovery magnitudes projected for the Rio Del Rey fields (6.7–9.2% OOIP for smart water at 3,000 mg/L) are broadly consistent with field-scale outcomes reported from comparable applications globally. The Clair Ridge field in the UK North Sea, operated by BP, reported incremental recovery of approximately 8% OOIP following low-salinity water flooding in low-permeability Devonian sandstones, while the Snorre field in Norway demonstrated 5–10% OOIP uplift in Triassic clastic reservoirs. In the West Africa context, the Angolan offshore Kwanza Basin pilots conducted by Total Energies reported 6–14% OOIP incremental recovery in Aptian siliciclastic reservoirs with broadly similar petrophysical and wettability characteristics to the Rio Del Rey sands.

The higher response magnitude in argillaceous facies (16.2% core-scale incremental recovery) compared to global sandstone averages for LSWF (typically reported as 5–15%

OOIP) reflects the unusually high clay CEC values observed in certain Rio Del Rey intervals, particularly in the Lokele deep Miocene sequence. This finding underscores the importance of lithofacies-targeted smart water design: injection strategies should prioritize sweep through clay-rich intervals while ensuring adequate coverage of all pay zones through appropriate well configuration.

Critical Design Parameters for Rio Del Rey Application

Integration of laboratory results and simulation sensitivities identifies five critical design parameters for smart water flooding in the Rio Del Rey context:

Injection Salinity Target: The optimal salinity window for maximum wettability alteration is 2,000–4,000 mg/L TDS, corresponding to approximately 7–10% of formation brine salinity. Below 1,500 mg/L, incremental recovery gains plateau while fines migration risk increases significantly. Above 5,000 mg/L, the EDL expansion effect weakens below the threshold needed for effective wettability modification.

SO_4^{2-} Concentration and SO_4^{2-}/Ca^{2+} Ratio: Elevated sulfate concentrations (800–2,200 mg/L) in the smart water formulation enhance wettability modification beyond pure salinity dilution effects. An SO_4^{2-}/Ca^{2+} molar ratio of 2.5–3.5 was identified as optimal based on contact angle response and core flood results. Sulfate is best supplied through partial nanofiltration rejection rather than chemical addition to control costs.

Injection Temperature Compatibility: At Rio Del Rey reservoir temperatures (75–100°C), sulfate precipitation as $CaSO_4$ (anhydrite) is a thermodynamic risk that must be managed through injection water scaling prediction and inhibitor programs. Simulations indicate that scaling risk is manageable within the 800–2,200 mg/L SO_4^{2-} range identified, provided Ca^{2+} is maintained below 150 mg/L.

Injection Timing (Secondary vs. Tertiary): Simulations consistently showed that early-stage smart water injection (commencing before conventional water breakthrough) outperforms tertiary application by 0.8–1.3% OOIP on an absolute basis, as the wettability alteration effect acts on a larger fraction of moveable oil.

Where fields are already in late waterflood stage, tertiary smart water application remains economically viable, particularly in zones where seawater injection has been limited.

Well Pattern and Injectivity Management: Line-drive patterns with alternating injector-producer rows perpendicular to the dominant permeability direction produced slightly better sweep efficiency than inverted five-spot patterns in the heterogeneous Rio Del Rey simulation model. Injectivity must be monitored closely during the salinity transition period to detect fines migration-induced impairment, with provision for temporary salinity increase ('salinity slug') protocols if injectivity decline exceeds 20%.

Water Source and Treatment Requirements

Rio Del Rey offshore operations have access to Atlantic seawater as the primary injection water source, supplemented by produced water re-injection (PWRI). Conversion from conventional seawater to smart water injection requires desalination treatment to reduce total salinity from ~35,000 mg/L to the target 3,000 mg/L range, which represents approximately 91% desalination. The most technically and commercially viable desalination technology for offshore application at this scale is reverse osmosis (RO), with nanofiltration (NF) as a potential pre-treatment step that simultaneously achieves partial desalination and sulfate rejection reversal (retaining sulfate-rich permeate while removing scale-forming divalent cations selectively).

A dedicated RO/NF treatment train with a capacity of 30,000–50,000 BWPD (equivalent to ~4,800–8,000 m^3/day) would be required per major producing field, representing the principal capital investment for smart water implementation. Power requirements for offshore RO at this capacity are estimated at 3–5 MW, manageable within existing generation capacity on the producing platforms. Produced water reuse represents an attractive complementary source: Rio Del Rey fields currently produce approximately 120,000 BWPD of formation water, which, after treatment to target salinity and ionic composition, could partially substitute for treated seawater in smart water blending schemes, potentially reducing desalination plant requirements by 30–40%.

Economic Analysis

Cost Framework

The economic evaluation considers capital expenditure (CAPEX) and operating expenditure (OPEX) for smart water implementation, discounted using a Weighted Average Cost of Capital (WACC) of 12% appropriate for a sub-Saharan offshore development context. Three oil price scenarios are evaluated: low (USD 50/bbl), base (USD 75/bbl), and high (USD 100/bbl). The production profiles from the P50 simulation realizations are used for NPV calculations.

ISSN No. 2454-6194 | DOI: 10.51584/IJRIAS |Volume XI Issue VI June 2026

Table 5: Capital and Operating Cost Estimates for Smart Water Implementation — Per Field

Cost Component	Unit	Kole Field	Moudi Field	Lokele Field
RO/NF Treatment Facility (CAPEX)	USD MM	45–65	35–55	40–60
Subsea Water Distribution Modifications	USD MM	12–22	10–18	11–20
Well Workover / Completion Modifications	USD MM	8–15	7–12	8–14
Monitoring & Surveillance Systems	USD MM	5–10	4–8	5–9
Total CAPEX (estimated)	USD MM	70–112	56–93	64–103
Annual OPEX — Water Treatment	USD MM/yr	8–14	6–11	7–13
Annual OPEX — Chemical Inhibitors	USD MM/yr	1.5–3	1.2–2.5	1.4–2.8
Total Annual OPEX	USD MM/yr	9.5–17	7.2–13.5	8.4–15.8

Net Present Value Analysis

NPV calculations over a 20-year project life (including 2–3 year implementation and ramp-up period) indicate positive economics under base and high oil price scenarios for all three fields.

Table 6: NPV Uplift from Smart Water Flooding versus Continued Seawater Injection

Field	Low Oil Price (USD 50/bbl)	Base Case (USD 75/bbl)	High Oil Price (USD 100/bbl)
Kole	USD -15 to +25 MM	USD +120 to +195 MM	USD +260 to +380 MM
Moudi	USD -22 to +10 MM	USD +85 to +145 MM	USD +190 to +290 MM
Lokele	USD -18 to +18 MM	USD +95 to +165 MM	USD +210 to +320 MM
Combined (P50)	USD -18 to +18 MM	USD +300 to +505 MM	USD +660 to +990 MM

The analysis reveals that smart water flooding is economically robust under base and high price scenarios, with combined NPV uplift of USD 300–505 million at USD 75/bbl and USD 660–990 million at USD 100/bbl across the three fields. The low oil price scenario yields marginally negative to modestly positive NPV, reflecting the capital intensity of offshore desalination facilities. Break-even oil price analysis indicates that the smart water program achieves positive NPV above approximately USD 58/bbl (P50 expectation), providing a sufficient economic buffer under current market conditions. The smart water plus polymer hybrid scenario shows NPV uplift 35–50% higher than smart water alone under base case conditions, but requires an additional USD 80–120 MM CAPEX per field for polymer handling facilities, raising the break-even price to USD 68/bbl.

Pilot Design And Implementation Roadmap

Based on the integrated technical and economic analysis, the following phased implementation approach is recommended for smart water flooding in the Rio Del Rey Basin:

Phase 1: Single-Well Pilot (Year 1–2)

Select one injector-producer pair in the Kole field (highest confidence geological model, existing metering

ISSN No. 2454-6194 | DOI: 10.51584/IJRIAS |Volume XI Issue VI June 2026

infrastructure). Install a small-scale RO unit (5,000 BWPD) to provide blended smart water at 3,000–5,000 mg/L. Monitor injectivity index, produced fluid ion composition, and oil cut weekly. Conduct regular traceable ion (Li^+ or Br^-) monitoring to differentiate smart water breakthrough from formation brine. Objective: validate smart water response under field conditions and calibrate simulation model.

Phase 2: Pattern Pilot (Year 3–5)

Expand to a three-injector, five-producer inverted five-spot pattern in the most responsive reservoir interval identified in Phase 1. Upscale RO facility to 20,000 BWPD. Introduce smart water with optimized ionic formulation ($SO4^{2-}/Ca^{2+}$ = 3.0). Implement a comprehensive dynamic data acquisition program including 4D seismic (if acquisition economics permit), production logging, and geochemical fluid sampling. Objective: confirm sweep efficiency improvement and production uplift at pattern scale.

Phase 3: Field-Scale Rollout (Year 6–15)

If pilot phases confirm economic recovery targets, implement full-field smart water flooding across all injector patterns in Kole, with parallel implementation programs initiated for Moudi and Lokele based on Phase 2 learnings. Scale RO/NF facilities to full capacity (30,000–50,000 BWPD per field). Integrate produced water reuse to reduce freshwater demand and operational cost. Ongoing surveillance and model updating to optimize injection salinity and rates in response to reservoir performance.

CONCLUSIONS

This comprehensive study of smart water flooding potential in the Rio Del Rey Basin yields the following principal conclusions:

The Rio Del Rey reservoir system, characterized by oil-wet to mixed-wet sandstones, high clay CEC, and saline formation water, presents highly favorable conditions for smart water flooding. Contact angle measurements confirmed wettability shift from 132° (oil-wet, formation brine) to 64° (near water-wet, optimized smart water) for representative core samples.

Core flooding experiments demonstrated incremental oil recovery of 9.7% OOIP (LSW at 5,000 mg/L) and 13.4% OOIP (optimized smart water at 3,000 mg/L) above conventional seawater injection baselines, with the highest response observed in clay-rich argillaceous sand facies (16.2% OOIP incremental for SW formulation).

Field-scale compositional simulation projects 6.7–9.2% OOIP incremental recovery over 15 years under optimized smart water injection, representing a 20–23% relative improvement over continued conventional seawater flooding. Early-stage smart water implementation provides an additional 0.8–1.3% OOIP uplift versus tertiary application.

The critical design parameters are injection water salinity (optimal target: 2,000–4,000 mg/L TDS), SO_4^{2-}/Ca^{2+} ratio (optimal: 2.5–3.5), injection timing, and fines migration management through controlled salinity transition protocols.

Economic analysis demonstrates positive NPV uplift of USD 300–505 million (combined across three fields) at USD 75/bbl base oil price, with a break-even price of approximately USD 58/bbl. The project is economically robust under base and high price scenarios and marginally economic at low prices, justifying phased implementation beginning with a single-well pilot.

Offshore RO/NF treatment systems are technically feasible and can be integrated with existing water handling infrastructure at a total CAPEX of USD 56–112 million per field. Produced water re use can reduce treatment capacity requirements by 30–40%.

A phased pilot-to-full-field implementation roadmap is recommended, commencing with a Kole single-well pilot in Year 1 to validate the technology under Rio Del Rey–specific field conditions before full-field commitment.

These findings collectively demonstrate that smart water flooding is a technically sound, economically attractive, and operationally feasible enhanced recovery strategy for the Rio Del Rey Basin. Successful implementation has the potential to unlock an additional 78–108 MMbbl of incremental oil production across the three study fields, making a material contribution to Cameroon's national hydrocarbon recovery goals and extending the productive life of this strategically important offshore province.

REFERENCES

1. Agbalaka, C.C., Dandekar, A.Y., Patil, S.L., Khataniar, S., & Hemsath, J.R. (2008). Coreflooding studies to evaluate the impact of salinity and wettability on oil recovery efficiency. Transport in Porous Media, 76(1), 77–94.
2. Al-Shalabi, E.W., & Sepehrnoori, K. (2016). Low salinity and engineered water injection for sandstone and carbonate reservoirs. Gulf Professional Publishing, Elsevier.
3. Austad, T., Rezaei-Doust, A., & Puntervold, T. (2010). Chemical mechanism of low salinity water flooding in sandstone reservoirs. SPE-129767-MS, Society of Petroleum Engineers.
4. Berg, S., Cense, A.W., Jansen, E., & Bakker, K. (2010). Direct experimental evidence of wettability modification by low salinity. Petrophysics, 51(5), 314–322.
5. Dang, C.T.Q., Nghiem, L.X., Nguyen, N.T.B., Chen, Z., & Nguyen, Q.P. (2016). Modeling and optimization of low salinity waterflood. Fuel, 173, 33–45.
6. Elakneswaran, Y., Shimokawara, M., Nawa, T., & Takahashi, S. (2017). Electrokinetics and wettability alteration in low salinity flooding. Energy & Fuels, 31(5), 4892–4900.
7. Fathi, S.J., Austad, T., & Strand, S. (2011). Smart water as a wettability modifier in chalk: the effect of salinity and ionic composition. Energy & Fuels, 25(6), 2514–2519.
8. Hognesen, E.J., Strand, S., & Austad, T. (2005). Waterflooding of preferentially oil-wet carbonates: oil recovery related to reservoir temperature and brine composition. SPE-94166-MS, Society of Petroleum Engineers.
9. Jerauld, G.R., Webb, K.J., Lin, C.Y., & Seccombe, J.C. (2008). Modeling low-salinity waterflooding. SPE Reservoir Evaluation & Engineering, 11(6), 1000–1012.
10. Lager, A., Webb, K.J., Black, C.J.J., Singleton, M., & Sorbie, K.S. (2008). Low salinity oil recovery — an experimental investigation. Petrophysics, 49(1), 28–35.
11. McGuire, P.L., Moritz, R.L., Flemings, P.B., & Harvey, A.H. (2005). Low salinity oil recovery: an exciting new EOR opportunity for Alaska's North Slope. SPE-93903-MS, Society of Petroleum Engineers.
12. Morrow, N.R., & Buckley, J. (2011). Improved oil recovery by low-salinity waterflooding. Journal of Petroleum Technology, 63(5), 106–112.
13. Nasralla, R.A., & Nasr-El-Din, H.A. (2014). Double-layer expansion: is it a primary mechanism of improved oil recovery by low-salinity water flooding? SPE Reservoir Evaluation & Engineering, 17(1), 49–59.
14. Nasralla, R.A., Sergienko, E., Masalmeh, S.K., van der Linde, H.A., Brussee, N.J., Mahani, H., Suijkerbuijk, B.M.J.M., & Alqallaf, A. (2018). Demonstrating the potential of low-salinity waterflooding and ozone treatment in carbonate reservoirs by single-well chemical tracer test. SPE Journal, 23(3), 736–752.
15. Rio Del Rey Development Operators Consortium (RDDOC). (2022). Rio Del Rey Basin Technical Review: Petrophysics, Reservoir Characterization and Production Performance Summary. Internal Technical Report TR-2022-04, Douala.
16. Sheng, J.J. (2014). Critical review of low-salinity waterflooding. Journal of Petroleum Science and Engineering, 120, 216–224.
17. Strand, S., Høgnesen, E.J., & Austad, T. (2006). Wettability alteration of carbonates — effects of potential determining ions (Ca^{2+} and SO_4^{2-}) and temperature. Colloids and Surfaces A, 275(1–3), 1–10.
18. Tang, G.Q., & Morrow, N.R. (1999). Influence of brine composition and fines migration on crude oil/brine/rock interactions and oil recovery. Journal of Petroleum Science and Engineering, 24(2–4), 99–111.
19. Teklu, T.W., Alameri, W., Graves, R.M., Kazemi, H., & AlSumaiti, A.M. (2016). Low-salinity water-alternating CO_2 EOR. Journal of Petroleum Science and Engineering, 142, 101–118.
20. Webb, K.J., Black, C.J.J., & Tjetland, G. (2005). A laboratory study investigating methods for improving oil recovery in carbonates. International Petroleum Technology Conference, IPTC-10506.